Particle-in-cell/Monte Carlo simulations of a low-pressure capacitively coupled radio-frequency discharge: Effect of adding H_2 to an Ar discharge

E. Neyts,[a] M. Yan, A. Bogaerts, and R. Gijbels
University of Antwerp, Department of Chemistry, Universiteitsplein 1, B-2610 Antwerp, Belgium

(Received 16 October 2002; accepted 4 February 2003)

A one-dimensional particle-in-cell/Monte Carlo code with three velocity components is developed to simulate a capacitively coupled radio-frequency Ar/H_2 discharge at low pressure, and to investigate the effect of adding hydrogen to an argon discharge. This self-consistent kinetic simulation technique allows one to study fundamental processes in the discharge at the molecular level. It is shown that the addition of small amounts of H_2 to an Ar discharge has profound effects on the discharge behavior, i.e., a change in the electron energy probability function, an increase in the electron density at low H_2 content and a decrease at higher H_2 content, as well as a dip in the Ar^+ ion density in the center of the discharge at higher pressure. These effects can be explained by the collision processes taking place in the discharge. The simulations were carried out in the pressure range 50–250 mTorr, at voltages of 300 and 800 V, while the H_2 content was varied between 0% and 10%, at a constant driving frequency of 13.56 MHz. © *2003 American Institute of Physics.* [DOI: 10.1063/1.1563820]

I. INTRODUCTION

Argon/hydrogen discharges are frequently used for surface cleaning purposes[1] and sputter-deposition processes.[2] Moreover, they are also a topic of interest for analytical applications.[3,4] It is stated that the presence of H_2 has a crucial influence on the discharge properties of an argon discharge.[5–14] An overview of the possible reactions in an Ar/H_2 discharge is given by Bogaerts.[8]

Experimentally, Mason *et al.*[9] studied the anomalous loss of ionization in an Ar/H_2 plasma by fast flow glow discharge mass spectrometry. The loss of ionization was attributed to the loss of highly excited Ar atoms, which are assumed to be the precursors for most of the ions. Ar/H_2 discharges were also investigated by Meulenbroeks *et al.*[10] in a cascaded arc plasma. They explain the loss of ionization as a result of molecular processes, such as the proton transfer between Ar^+ and H_2 yielding ArH^+, followed by an efficient recombination reaction between electrons and ArH^+. Electron energy distribution functions (EEDFs) have been measured experimentally for Ar/H_2 capacitively coupled discharges (CCDs) by Müller.[7] Ion energy distribution functions in Ar/H_2 mixtures were measured in a planar inductive discharge by Gudmundsson[11] and in CCDs by Manenschijn *et al.*,[12] Radovanov *et al.*,[13] and Djurovic.[14]

Argon/hydrogen discharges have not been modeled extensively yet; in literature, a hybrid Monte Carlo—fluid model[5,6] for a direct current glow discharge and a model based on particle balance equations for a thermal plasma[15] can be found.

In this article, we study the influence of small amounts of hydrogen in an Ar capacitively coupled rf discharge for different pressures, voltages, and partial hydrogen pressures, in order to gain a better understanding of the dynamics of this kind of discharge. A better understanding of the discharge behavior is imperative to improve the existing applications. Particle-in-cell (PIC) and particle-in-cell/Monte Carlo (PIC-MC) simulations have been used extensively to study the fundamental processes in CCDs,[16–29] but to the authors' knowledge, no attempt has been made so far to model an Ar/H_2 discharge by PIC-MC simulations. The different discharge behavior, observed between a pure Ar discharge and an Ar/H_2 discharge, can be explained in terms of the collision processes in the plasma. In Sec. II, the model will be briefly described, whereas Sec. III will deal with the results. Finally, a summary and conclusion will be given in Sec. 4.

II. THE PARTICLE-IN-CELL/MONTE CARLO MODEL FOR Ar/H_2 DISCHARGES

A. Basics of a particle-in-cell/Monte Carlo model

In the PIC method, so-called ''superparticles'' move in the discharge space through an artificial grid on a timestep basis. Each of these superparticles represents typically about 10^8 real particles. Only charged particles are simulated with these superparticles; neutrals are assumed to form a continuum. In the beginning of the simulation, every charged particle is assigned to a specific position on the grid, leading to a self-generated electric field. A certain potential is applied at one of the electrodes, giving rise to the applied electric field. The particles move in response to both the applied and self-generated fields, according to Newton's laws. This gives rise to positions for the particles, changing the self-created field, and hence changing the force acting on the particles. Mathematically, this is done every timestep by first *weighting* the positions of the particles to the grid, yielding the charge densities on the grid points. The potential and electric field on the grid points are then determined from the calcu-

[a]Electronic mail: erik.neyts@ua.ac.be

lated charges, by Poisson's equation. A weighting procedure is applied again, to obtain the forces on the positions of the particles from the previously obtained field on the grid points. From the force on the positions of the particles, first, the velocity of every particle is calculated and, from the velocity, the position is determined, using a modified leap-frog algorithm. After the particles are placed in their positions, a Monte Carlo algorithm is used to simulate collisions between particles. Both charged–neutral particle collisions and charged–charged particle collisions are considered. This procedure is repeated for many timesteps, until convergence is reached.

In the MC module, a random number between 0 and 1 is chosen to determine for every particle whether or not a collision occurs. If a collision takes place, a second random number is generated to determine the collision type. The energy and direction of the particles after the collision are determined, depending on the collision type, again using random numbers. We make use of the ''null-collision'' method.[19] In this approach, a ficticious collision process (null-collision) is introduced, with a collision frequency such that when it is added to the sum of the collision frequencies of the real collision processes, a constant total collision frequency over position and energy is obtained. In this way, the maximum fraction of the total number of particles in the simulation that undergo a collision (either a real or a null collision) during a timestep Δt, is given by

$$P_{\text{null}} = 1 - \exp(-\nu' \Delta t), \tag{1}$$

where

$$\nu' = \max_{x,\epsilon}(n_t \sigma_T \nu) = \max_{x}(n_t) \max_{\epsilon}(\sigma_T \nu). \tag{2}$$

In Eq. (2), the subscripts under max denote the quantaties over which the maximum is taken. In Eq. (2), x denotes the position, ϵ is the energy of the incident particle, n_t is the density of the incident particles, σ_T is the total cross section for every species, and ν is the velocity of the incident particle. However, this implies that the density of the target particles is constant in space. This means that the approach can only be used when the target particles are neutral gas molecules, which are assumed in our model to be uniformly distributed throughout the discharge volume. In this procedure, the collision probability must be calculated only once, instead of every timestep. This avoids looking up the kinetic energy of each particle at every timestep, thus speeding up the code.

Another speeding-up procedure used in the code is to apply different timesteps for ions and electrons. Since ions move much more slowly in the electric field, due to their larger mass, a larger timestep can be used, e.g., one ion timestep is equal to ten electron timesteps. A description of different speeding up procedures for PIC-MC simulations can be found in Ref. 30. A more thorough description of the PIC method can be found in Birdsal and Langdon.[31] The basic ideas of PIC-MC are given in more detail by Vahedi.[19,32]

B. Particle-in-cell-Monte Carlo model for the Ar/H_2 discharge

A PIC-MC model is developed to simulate an Ar/H_2 discharges. The MC module is based on the model of Vahedi and Surendra.[19] Our model takes into account five differently charged particle species, i.e., electrons, Ar^+ ions, ArH^+ ions, H_2^+ ions, and H_3^+ ions. H atoms and H^+ ions are not taken into account, due to their very low densities. This approximation is only valid if the dissociation degree of H_2 is sufficiently low, which is indeed expected at the conditions under study.[5] Furthermore, excited atoms and molecules are also not followed as particles. Therefore, excitation reactions serve only as an effective energy sink for the electrons.

The atoms and molecules are assumed to be uniformly distributed throughout the discharge space, with a Maxwellian velocity distribution at a gas temperature of $T_{\text{gas}} = 0.026\,\text{eV}\,(300\,\text{K})$. Since in these discharges the ionization degree is fairly low ($\sim 10^{-6}$), and since also the dissociation degree for H_2 is low enough,[5] all neutrals are given a predefined density which remains fixed throughout the time evolution of the discharge.

The reactions taken into account in the model are given in Table I; the choice of reactions was based on the overviews given by Bogaerts.[5,8] It must be mentioned that no rotational excitation reactions of H_2 were incorporated in the model, since the threshold for these reactions is very low. Therefore, we assume that the energy loss of the electrons due to these reactions will be negligible. The separation between elastic scattering and symmetric charge transfer of Ar^+ ions with Ar atoms (see Table I) is purely artificial, and is introduced since it parallels collisions between nonidentical particles,[19] e.g., between argon ions and hydrogen molecules.

The three recombination reactions are treated as electron impact collisions. However, since the target species in these reactions (H_2^+, H_3^+, or ArH^+) do not have a uniform density distribution in the discharge, these reactions can only be modeled by the null-collision procedure, when taking into account the dependence of the total collision frequency on the position-dependent density of the target species. Instead, we chose to model these reactions making use of reaction rate constants.

III. RESULTS

The simulations are carried out for a discharge cell with two parallel equal electrodes, and an interelectrode distance $d = 2.5\,\text{cm}$. Calculation results will be presented for discharge voltages of 300 V and 800 V, and pressures in the range 50–250 mTorr. The hydrogen concentration is varied between 0% and 10%. The electron energy probability functions (EEPFs) presented next were calculated in the middle of the discharge.

A. Electron energy probability function

The EEPF is defined as

$$f(\epsilon) = F(\epsilon) \cdot \epsilon^{-1/2}, \tag{3}$$

TABLE I. Reactions taken into account in the model, and references from which the cross sections or reaction rate constants were adopted.

Reaction	Reaction type	Reference No.
$e+\mathrm{Ar} \rightarrow e+\mathrm{Ar}$	elastic scattering	33
$e+\mathrm{Ar} \rightarrow e+\mathrm{Ar}^*$	excitation	33
$e+\mathrm{Ar} \rightarrow 2e+\mathrm{Ar}^+$	ionization	33
$e+\mathrm{H_2} \rightarrow e+\mathrm{H_2}$	elastic scattering	34
$e+\mathrm{H_2} \rightarrow e+\mathrm{H_2^*}(v)$	vibrational excitation	34
$e+\mathrm{H_2} \rightarrow e+\mathrm{H_2^*}(s)$	singlet excitation	34
$e+\mathrm{H_2} \rightarrow 2e+\mathrm{H_2^+}$	ionization	34
$e+\mathrm{H_2} \rightarrow e+\mathrm{H_2^*}(t) \rightarrow e+2\mathrm{H}$	triplet excitation, followed by dissociation	34
$e+\mathrm{H_2^+} \rightarrow 2\mathrm{H}$	recombination	35
$e+\mathrm{H_3^+} \rightarrow \mathrm{H}+\mathrm{H_2}$	recombination	35
$e+\mathrm{ArH^+} \rightarrow \mathrm{H}+\mathrm{Ar}$	recombination	35
$\mathrm{Ar^+}+\mathrm{Ar} \rightarrow \mathrm{Ar^+}+\mathrm{Ar}$	elastic scattering	19
$\mathrm{Ar^+}+\mathrm{Ar} \rightarrow \mathrm{Ar}+\mathrm{Ar^+}$	symmetric charge transfer	19
$\mathrm{Ar^+}+\mathrm{H_2} \rightarrow \mathrm{Ar}+\mathrm{H_2^+}$	charge transfer	36
$\mathrm{Ar^+}+\mathrm{H_2} \rightarrow \mathrm{ArH^+}+\mathrm{H}$	H-atom transfer	36
$\mathrm{H_2^+}+\mathrm{H_2} \rightarrow \mathrm{H_2}+\mathrm{H_2^+}$	symmetric charge transfer	37, 38
$\mathrm{H_2^+}+\mathrm{H_2} \rightarrow \mathrm{H_3^+}+\mathrm{H}$	proton transfer	37, 38
$\mathrm{H_2^+}+\mathrm{Ar} \rightarrow \mathrm{ArH^+}+\mathrm{H}$	proton transfer	36, 39
$\mathrm{H_2^+}+\mathrm{Ar} \rightarrow \mathrm{H_2}+\mathrm{Ar^+}$	charge transfer	36, 39
$\mathrm{H_3^+}+\mathrm{Ar} \rightarrow \mathrm{H_3^+}+\mathrm{Ar}$	elastic scattering	36, 39, 40
$\mathrm{H_3^+}+\mathrm{Ar} \rightarrow \mathrm{ArH^+}+\mathrm{H_2}$	proton transfer	36, 39, 40
$\mathrm{H_3^+}+\mathrm{Ar} \rightarrow \mathrm{H^+}+\mathrm{H_2}+\mathrm{Ar}$	collision-induced dissociation	36, 39, 40
$\mathrm{ArH^+}+\mathrm{Ar} \rightarrow \mathrm{ArH^+}+\mathrm{Ar}$	elastic scattering	39
$\mathrm{ArH^+}+\mathrm{H_2} \rightarrow \mathrm{ArH^+}+\mathrm{H_2}$	elastic scattering	39
$\mathrm{ArH^+}+\mathrm{H_2} \rightarrow \mathrm{H_3^+}+\mathrm{Ar}$	proton transfer	39

where $F(\epsilon)$ is the EEDF, and ϵ is the electron energy. The EEPF is normalized such that the integral over the energy equals 1. The EEPF is plotted instead of the EEDF to easily distinguish between Maxwellian, bi-Maxwellian, and Druyvenstein-type energy distributions. In a PIC-MC simulation, no assumptions have to be made according to the EEDF, and the latter arises naturally from the discharge dynamics. Therefore, the resulting EEDF is generated self-consistently. The EEPFs that are presented here were calculated in the bulk of the discharge. In the sheaths, deviant distributions are formed (not shown).

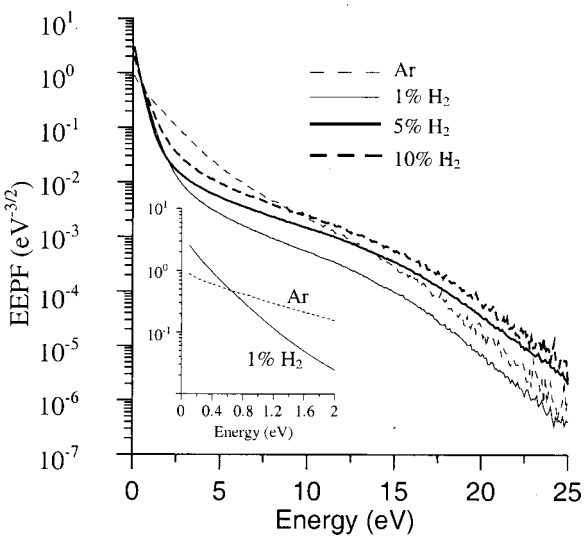

FIG. 1. Calculated EEPF for argon (dashed line), and admixtures of 1% H_2 (solid line), 5% H_2 (thick solid line), and 10% H_2 (thick dashed line), at 300 V and 100 mTorr. The inset is a magnification of the very low-energy part for argon (dashed line) and the Ar/1% H_2 mixture (solid line).

In Fig. 1, the EEPFs are shown for a discharge at 300 V at a pressure of 100 mTorr, for pure argon, and for Ar/H_2 mixtures with 1%, 5%, and 10% H_2 content. It can be seen that the Ar/H_2 discharges exhibit a more bi-Maxwellian behavior than the pure Ar case, and that the difference between the Ar and the Ar/H_2 discharges is the largest at the lowest H_2 content. It appears also (from the inset in Fig. 1) that the fraction of very low-energy electrons (with energies smaller than about 0.8 eV) is increased in the Ar/H_2 cases in comparison with the pure Ar case, and the increase is larger for the lowest H_2 content investigated. On the other hand, the fraction of electrons with energies in the range 1–8 eV is lower in the Ar/H_2 cases than in the pure argon case. At even higher energies, the fraction of electrons with a certain energy again becomes higher than in the Ar case, and this also seems to be related to the percentage of H_2 added. As more H_2 is added, the fraction of electrons above a certain energy becomes higher than in the Ar case at lower energy ($\sim$8.5 eV for 10% H_2, $\sim$12.5 eV for 5% H_2, and at about 35 eV for the 1% H_2 case, not visible on this scale).

These phenomena can be explained as follows. A bi-Maxwellian energy distribution is usually attributed to stochastic electron heating in the rf sheaths, and in argon, it is enhanced by the Ramsauer effect.[41] This mechanism for electron heating is most significant at low pressure, whereas at higher pressure, electrons will be heated mainly collisionally, yielding a Druyvenstein-type distribution. The increase in very low energetic electrons in the Ar/H_2 mixtures is due

to the very low vibrational excitation threshold for H_2 at 0.54 eV, serving as an effective energy loss for electrons with energies somewhat above this threshold. When adding more H_2, this effect becomes more important, since the probability for this reaction increases. On the other hand, upon adding more H_2, the fraction of argon atoms decreases, so that also the Ramsauer effect becomes smaller. These two effects oppose each other. It is expected that at lower H_2 content, where the Ramsauer effect is still significant, the excitation reaction is predominant, leading to a strong increase in very low-energy electrons, while at higher H_2 content, the decreasing Ramsauer effect somewhat reduces the effect of the excitation reaction, so that there is still an increase in the fraction of very low-energy electrons compared to the pure argon case, but to a lesser extent.

The inflexion points of the EEPFs in the Ar/H_2 discharge at low energy are situated around 2.5 eV, around the energy for which this vibrational excitation reaction has a maximum in its cross section. Therefore, the fraction of electrons with energies in the range 1–8 eV is lower in the Ar/H_2 cases than in the pure argon case. This explains why the EEPFs are more bi-Maxwellian type than the EEPF of pure Ar. Indeed, the fraction of electrons with an energy below 2.5 eV increases more rapidly with decreasing energy than in the Ar case because of the important vibrational exitation reaction.

Further, the fraction of electrons in the Ar/H_2 mixtures at higher energy again becomes higher than the fraction of electrons in the argon discharge, and this occurs at increasing energy for decreasing H_2 content, as mentioned before. This can be explained by looking at the reaction rates for those reactions with a high threshold energy: Ionization and excitation of argon, and ionization and singlet excitation of hydrogen. Ionization and singlet excitation of H_2 only play a minor role as an energy loss mechanism for the electrons as compared to the electron energy loss due to ionization and excitation of argon. However, both excitation and ionization of argon decrease upon the addition of H_2. Therefore, a smaller fraction of the high-energy part of the electrons loses energy in these processes, so that more electrons with high energy retain their energy, eventually leading to a higher fraction of high-energy electrons than in the argon case. Finally, the behavior of the EEPF at high energy is also a direct consequence of the behavior at lower energy, and of the fact that the EEPFs are normalized to 1.

When turning to higher pressure, Fig. 2 shows that instead of a bi-Maxwellian distribution, the EEPF's are now formed more Druyvenstein type, since the discharge will be more dominated by collisions. As a result, the order of the high-energy tails for these cases should be more apparent. Indeed, Fig. 2 (for 250 mTorr) shows, more clearly than in Fig. 1, a higher fraction of high-energy electrons for the Ar/H_2 mixtures than for pure argon. This relative big difference in the fraction of the high-energy electrons is also attributed to the increased dissipated power with increased H_2 content, for the same applied voltage. This might also explain why the fraction of low-energy electrons (lower than 2 eV) lowers, as more H_2 is added (see Fig. 2). The EEPFs shift toward the higher-energy direction.

Turning now to a higher applied voltage of 800 V at low pressure of 100 mTorr, as shown in Fig. 3 for pure argon, 1% and 10% added H_2, again the influence of adding H_2 is clearly visible. When comparing with the 300 V case, the power dissipated in the discharge increases by an order of magnitude, as does the electron density, while the average electron energy slightly decreases. The distributions, however, do not differ much from the 300 V case: in all cases a bi-Maxwellian distribution is formed, being more pronounced in the $Ar/10\%\ H_2$ case, and somewhat less pronounced in the $Ar/1\%\ H_2$ case.

When comparing EEPFs for different pressures, as is shown in Fig. 4 for pure argon and in Fig. 5 for $Ar/1\%\ H_2$, it can be seen that the evolution from a bi-Maxwellian dis-

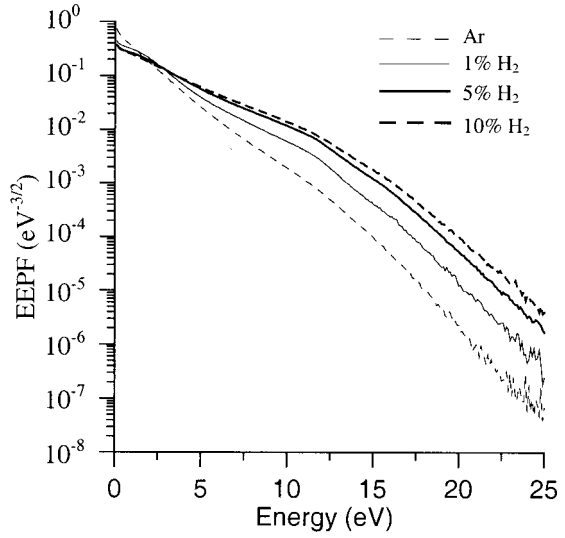

FIG. 2. Calculated EEPF for argon (dashed line), and admixtures of 1% H_2 (solid line), 5% H_2 (thick solid line), and 10% H_2 (thick dashed line), at 300 V and 250 mTorr.

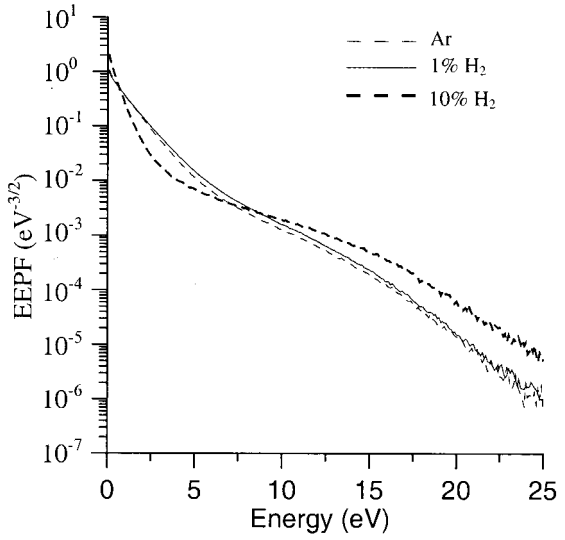

FIG. 3. Calculated EEPF for pure argon (dashed line), and admixtures of 1% H_2 (solid line), and 10% H_2 (thick dashed line), at 800 V and 100 mTorr.

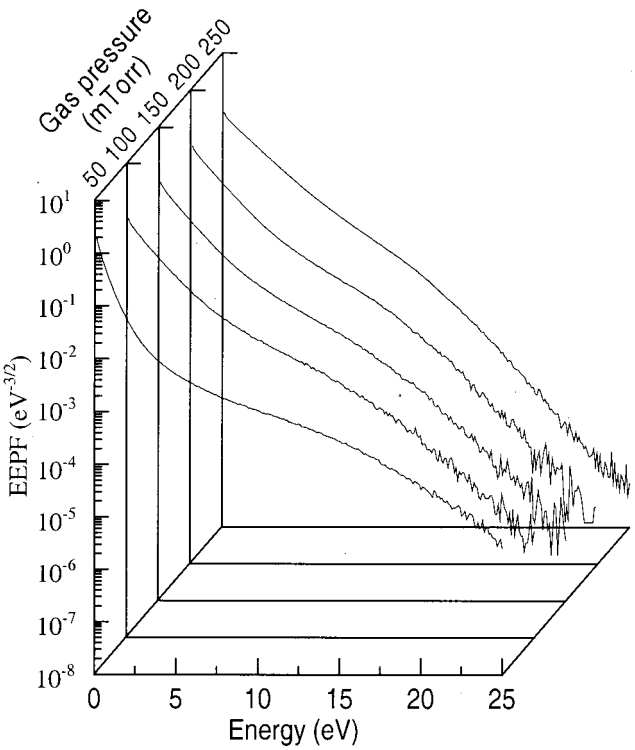

FIG. 4. Calculated EEPF for argon at different pressures at 300 V.

tribution to a Maxwellian one occurs already at lower pressure in pure argon than when hydrogen is added. This indicates that the addition of hydrogen favors the formation of a bi-Maxwellian distribution, which has already been explained. It is also clear that at low levels of H_2 content (in this case 1%), the reduction of the Ramsauer effect is negligible.

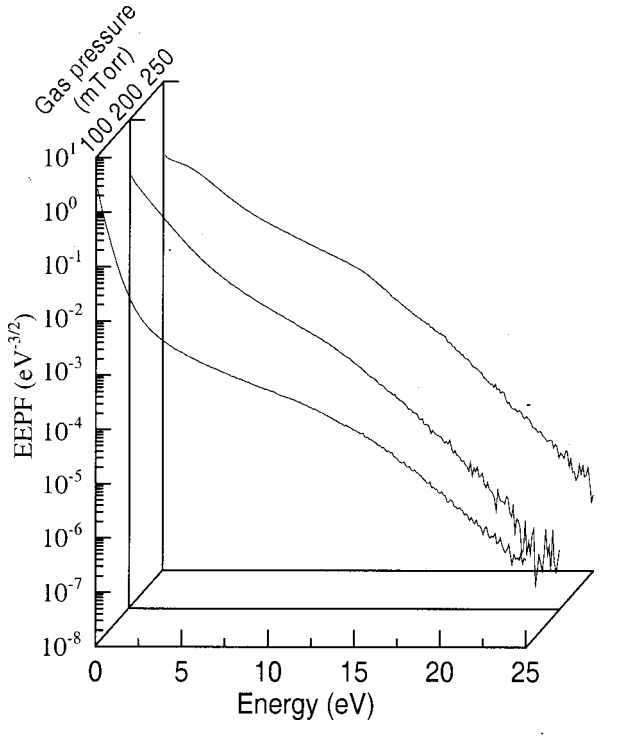

FIG. 5. Calculated EEPF for the Ar/1% H_2 mixture at different pressures at 300 V.

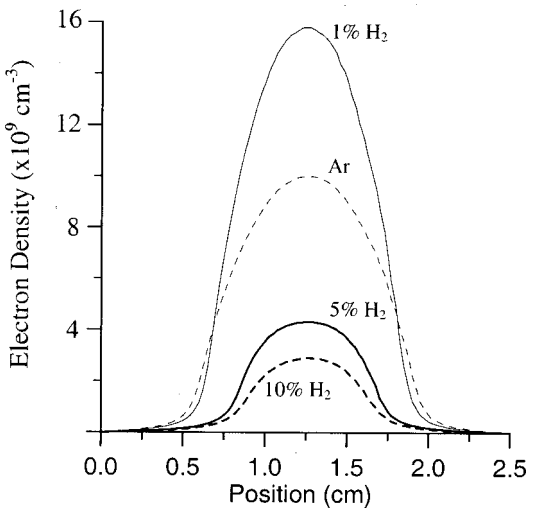

FIG. 6. Calculated time-averaged electron density profiles for pure argon (dashed line), and admixtures of 1% H_2 (solid line), 5% H_2 (thick solid line) and 10% H_2 (thick dashed line), at 300 V and 100 mTorr.

B. Density profiles

In Figs. 6 and 7, the time-averaged electron density profiles are shown for an applied voltage of 300 V and pressures of 100 mTorr and 250 mTorr, respectively, for pure argon, and admixtures of argon with 1%, 5%, and 10% H_2. The EEPFs of these discharges were shown in Figs. 1 and 2, respectively. In literature, it was already demonstrated that the additions of hydrogen to an argon discharge lowers the electron density.[9,10] This phenomenon is also confirmed by our results for all admixtures, except for the case with 1% H_2 at 100 mTorr and 300 V. For adding only 1% H_2 at 100 mTorr and 300 V, our model predicts that the electron density increases instead of decreases relative to the pure argon discharge.

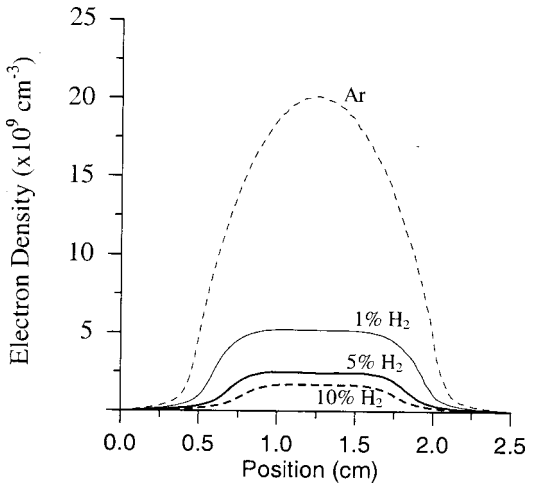

FIG. 7. Calculated time-averaged electron density profiles for pure argon (dashed line), and admixtures of 1% H_2 (solid line), 5% H_2 (thick solid line) and 10% H_2 (thick dashed line), at 300 V and 250 mTorr.

We believe that the reason for this increase in electron density at 100 mTorr when adding 1% of H_2 as compared to the pure argon discharge, can be found in the EEPF (Fig. 1). Indeed—as explained herein—the fraction of very low-energy electrons is higher than in the pure argon case by a factor of about 2–3, while the fraction of higher-energy electrons is lower. Therefore, upon the addition of 1% H_2, the number of electrons being ''captured'' in the middle of the discharge increases as compared by the pure argon case, leading to a reduced loss of electrons at the walls.

As far as the decrease in electron density upon the addition of H_2 is concerned, it was previously attributed in literature to the so-called ''loss of ionization''. This loss of ionization was explained Meulenbroeks[10] by a combination of two reactions; i.e., H-atom transfer:

$$(1) \quad Ar^+ + H_2 \rightarrow ArH^+ + H,$$

followed by an efficient recombination reaction

$$(2) \quad ArH^+ + e^- \rightarrow Ar + H^*,$$

while Mason[9] assumed this loss of ionization to be due to a decrease in the density of highly excited metastable levels of Ar, which would be the precursors for most ions.

However, in our simulations, this loss of ionization cannot be explained by the first mechanism, since reaction (2) is found to be negligible for the conditions under study, contributing to the electron loss for less then 1% at the conditions under study. Also the second mechanism cannot explain our results, since metastables are not included in the model.

We believe that the decrease in electron density in our case can be found by looking at the relative importance of several reactions. The aforementioned reaction (1) is the main mechanism for the formation of ArH^+ ions (~84% at 100 mTorr and ~80% at 250 mTorr, almost independent of the H_2 content), and also an important mechanism for the loss of Ar^+ ions at 100 mTorr when more than 1% of H_2 is added. At 100 mTorr and 1% added H_2, this reaction is responsible for only 24% of the Ar^+ loss, which is low compared to when 5% H_2 is added (62%) and 10% H_2 added (64%). Also, at 250 mTorr, this reaction is the main mechanism for Ar^+ loss: 56% at 1% added H_2, 75% at 5% added H_2 and 81% at 10% added H_2.

When more than 1% hydrogen is added at 100 mTorr, or for all hydrogen contents at higher pressure, the ion–molecule reactions become much more important (as can also be seen in the ion densities, see next). Under these conditions, the positive charge is now not only preserved by an ionization process creating also electrons, but also by ion–molecule reactions. Both ArH^+ and H_3^+, providing a significant contribution to the total positive charge, cannot be created by ionization. Only three mechanisms are possible to explain the decrease in electron density as H_2 is added: (1) recombination of electrons with ions, (2) a decrease in the ionization rate, and (3) increased electron loss at the walls. It turns out that the recombination reactions play only a very minor role in the discharge, responsible for less than 1% of the electron loss under all circumstances. From our simulation results, we conclude that both (2) and (3) are correct: There is a decrease in the ionization rate of argon when adding H_2 (this is the only reaction which creates a substantial amount of electrons), as well as a increase in the loss of electrons at the walls.

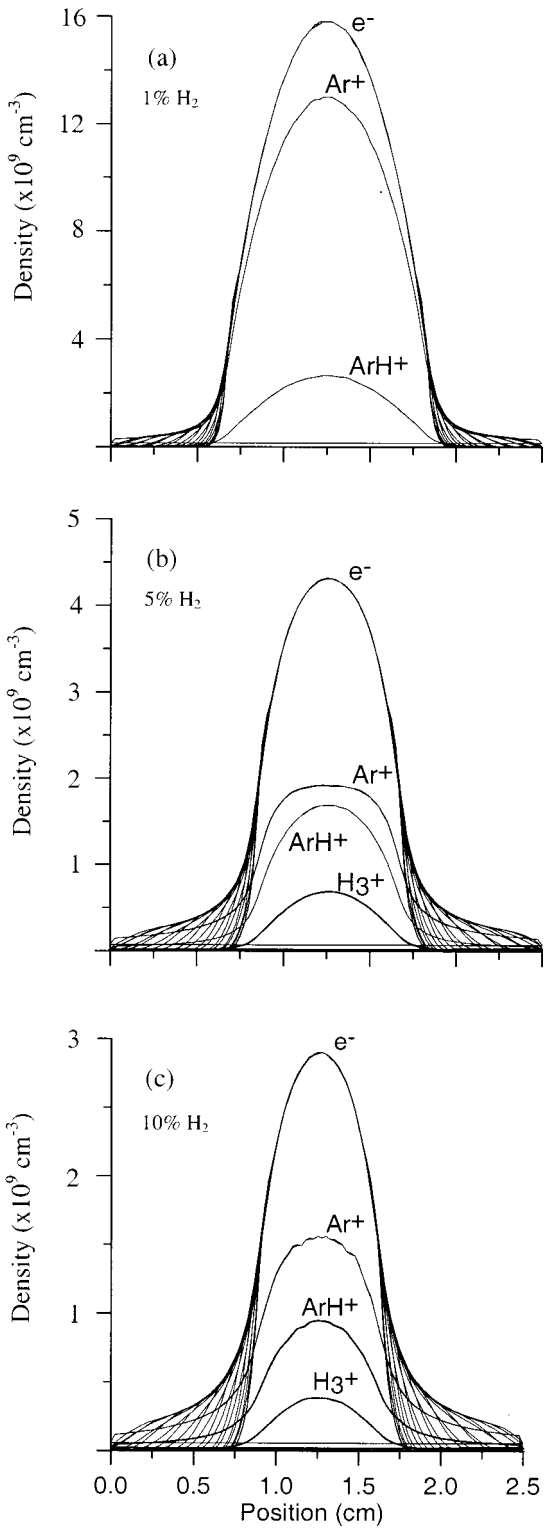

FIG. 8. Calculated electron and ion density profiles at 300 V and 100 mTorr for (a) the Ar/1% H_2 mixture, (b) the Ar/5% H_2 mixture, and (c) the Ar/10% H_2 mixture.

The effect of the addition of hydrogen is also clear in the ion density profiles, as shown in Figs. 8(a)–8(c) for 300 V, 100 mTorr, and 1%, 5%, and 10% added hydrogen, respec-

tively. At low hydrogen concentration (1%), the main ion remains Ar^+, while ArH^+ is of minor importance. The other positive ions (H_2^+ and H_3^+) are negligible. Upon the addition of more hydrogen [5% and 10%, Figs. 8(b) and 8(c)], it becomes clear that the ion–molecule reactions now dominate the discharge, so that Ar^+ and ArH^+ almost reach the same density. Also, the presence of H_3^+—which can only be created by ion–molecule reactions—becomes important for the maintenance of electroneutrality, having a maximum density only about 2.5 times lower than ArH^+. The H_2^+ density under these conditions is still negligible having a maximum density of about $10^{13}\,m^{-3}$, i.e., two orders of magnitude lower than the other ions. These observations are consistent with the increasing importance of the ion–molecule reactions, altering the charge buildup and preservation in the discharge. At this low pressure (100 mTorr), all species still have their maxima in the middle of the discharge.

When turning now to higher pressure (250 mTorr) at 300 V, for 1%, 5%, and 10% added hydrogen, as shown in Figs. 9(a)–9(c) respectively, an important change in this behavior is observed. Even at the lowest content of H_2 investigated (1%), ArH^+ becomes important for preserving electroneutrality, having a maximum density about half of the Ar^+ density. The most remarkable effect however is the shift of the maximum Ar^+ density from the middle of the discharge toward the edges of the sheaths. The depletion of Ar^+ ion density in the middle of the discharge is accompanied by a maximum in the ArH^+ and H_3^+ densities. Since the maximum of the Ar^+ ion density is no longer in the middle of the discharge, the sum of the ion densities becomes a plateau instead of a real maximum. Because the total ion density in the bulk of the discharge should be equal to the electron density due to electroneutrality, this results in a flat-shaped electron density profile in the middle of the discharge. We believe that this effect is a consequence of the formation mechanism of the different species. Ar^+ is created for more than 95% by electron impact ionization of Ar, occurring in the sheaths and the sheath boundaries. Therefore, the Ar^+ ion density develops initially there. On the other hand, ArH^+ is created mainly from Ar^+, with a rate nearly independent of the position in the bulk of the discharge. Indeed, the Ar^+ density reaches its maximum near the sheath boundaries, but the Ar^+ energy is also higher here than in the bulk of the discharge. Since the cross section for the reaction creating ArH^+ decreases rapidly with increasing energy, both effects compensate for each other and the formation rate of ArH^+ becomes nearly independent of position. This leads to a maximum of the ArH^+ ions in the middle of the discharge, due to diffusion and migration. Indeed, the depletion of the charge in the middle of the discharge creates an electric field which pushes the other positive ions toward the middle. Because charge neutrality is preserved in this way, the Ar^+ ion density can only develop at the sheath boundaries, where it is created. The proton transfer reaction, between ArH^+ and H_2, forming H_3^+ ions, has a rate which is constant in the bulk of the discharge. Again, a maximum is formed in the middle of the discharge due to diffusion and migration. H_2^+ on the other hand is formed almost entirely out of Ar^+ and H_2 by a charge transfer reaction, which has a rate with maxima near the electrodes, and a minimum in the middle of the discharge. Therefore, the H_2^+ density will also have maxima located near the sheaths of the discharge.

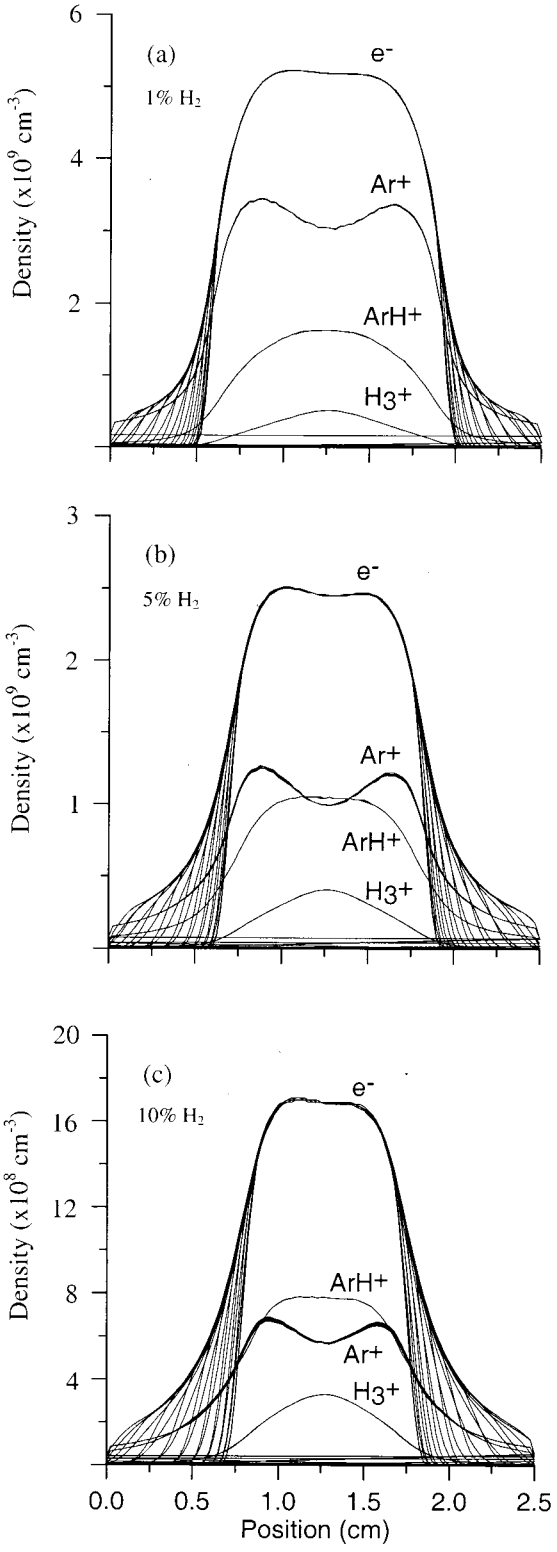

FIG. 9. Calculated electron and ion density profiles at 300 V and 250 mTorr for (a) the Ar/1% H_2 mixture, (b) the Ar/5% H_2 mixture, and (c) the Ar/10% H_2 mixture.

When adding more hydrogen, the importance of the ion–molecule reactions increases, so that at 5% H_2, the density of the ArH^+ ion becomes comparable to Ar^+ and at 10% H_2

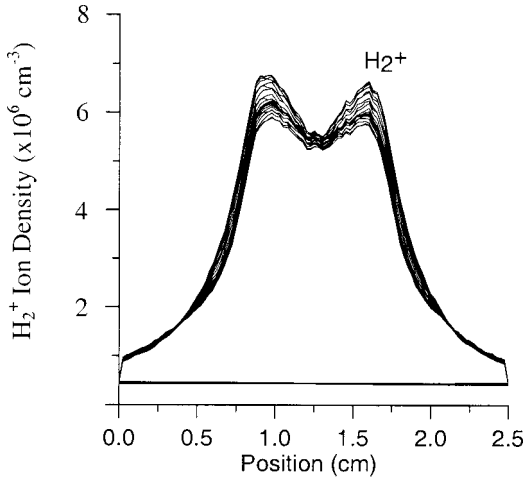

FIG. 10. Calculated H_2^+ ion density profile for the Ar/1% H_2 mixture at 300 V and 250 mTorr.

the ArH^+ density becomes even higher than the Ar^+ density. However, the shapes of the profiles are the same as for 1% H_2 addition. The results are shown in Figs. 9(b) and 9(c) for 5% and 10% H_2, respectively.

Finally, Fig. 10 shows the H_2^+ ion density at 300 V and 250 mTorr for 10% H_2 addition. Since H_2^+ is created mainly from Ar^+ in a strongly phase-dependent way, the density of the H_2^+ ions follows the phase dependence of its main creation reaction. This results in the strong phase dependence of the H_2^+ ion density profile shown in Fig. 10.

IV. SUMMARY AND CONCLUSION

In this work, capacitively coupled rf discharges in argon and argon/hydrogen mixtures with varying amounts of hydrogen were investigated at different pressures, in order to gain a better understanding of the discharge dynamics. Special attention has been paid to the various density profiles, both for the electrons and the ions, as well as to the EEPF. We found that in most cases, the electron density in the Ar/H_2 discharge is lower than in the pure Ar discharge, as was previously demonstrated by experimental results. This phenomenon can be explained for the conditions under study as a result of a lower ionization rate of argon, more electron loss at the walls, and the ion–molecule reactions which dominate the discharge. However, at a pressure of 100 mTorr, an applied voltage of 300 V and 1% of H_2, we found an increase in the electron density relative to the pure argon discharge under the same conditions. This is explained by the difference in the EEPF relative to the argon case (in agreement with experimental work), providing a much larger fraction of low-energy electrons, and by a minor influence of the ion–molecule reactions under these conditions, as exemplified by the ion density profiles. Also, changes in the EEPF due to the addition of hydrogen have been observed and explained. The formation of a bi-Maxwellian EEPF at low pressure, is favored by the addition of H_2 to the argon discharge, due to the vibrational excitation reaction of hydrogen at very low energy.

At higher pressure, the dissipated power due to electron collisions increases, leading to a more pronounced Druyvenstein-type distribution as compared to the pure argon discharge under the same conditions. The electron density profile now exhibits a plateau-shaped profile, as a consequence of the corresponding ion densities: ArH^+ and H_3^+, both formed by ion–molecule reactions, have their maxima in the middle of the discharge, while Ar^+ and H_2^+ have their maxima near the sheaths. Since the sum of the positive ion densities must equal the electron density in the bulk of the discharge due to electroneutrality, a plateau-shaped electron density profile results.

ACKNOWLEDGMENTS

One of the authors (E.N.) is indebted to the Institute for the Promotion of Innovation by Science and Technology in Flanders (IWT-Flanders) for financial support. Another author (A.B.) is indebted to the Flemish Fund for Scientific Research (FWO-Flanders) for financial support. Another author (M.Y.) acknowledges financial support from a ''Bilateral Scientific and Technological Cooperation'' project between Flanders and China (BIL 99/46). The authors also acknowledge financial support from the Federal Services for Scientific, Technical, and Cultural Affairs (DWTC/SSTC) of the Prime Minister's Office through IUAP-V.

[1] C. V. Budtz-Jorgensen, P. Kringhoj, and J. Bottiger, Surf. Coat. Technol. **938**, 116 (1999).
[2] H. Takahashi, H. Nagata, and H. Kataoka, Thin Solid Films **227**, 132 (1996).
[3] V. D. Hodoroaba, V. Hoffmann, E. B. M. Steers, and K. Wetzig, J. Anal. At. Spectrom. **15**, 1075 (2000).
[4] V. D. Hodoroaba, V. Hoffmann, E. B. M. Steers, and K. Wetzig, J. Anal. At. Spectrom. **15**, 951 (2000).
[5] A. Bogaerts and R. Gijbels, Spectrochim. Acta, Part B **57**, 1071 (2002).
[6] A. Bogaerts and R. Gijbels, Phys. Rev. E **65**, 056402 (2002).
[7] M. Müller, M. Sc. thesis, University Essen, 1997.
[8] A. Bogaerts and R. Gijbels, J. Anal. At. Spectrom. **15**, 441 (2000).
[9] R. S. Mason, P. D. Miller, and I. P. Mortimer, Phys. Rev. E **55**, 7462 (1997).
[10] R. F. G. Meulenbroeks, A. J. van Beek, A. J. G. van Helvoort, M. C. M. van de Sanden, and D. C. Schram, Phys. Rev. E **49**, 4397 (1994).
[11] J. T. Gudmundsson, Plasma Sources Sci. Technol. **8**, 58 (1999).
[12] A. Manenschijn, G. C. A. M. Janssen, E. van der Drift, and S. Radelaar, J. Appl. Phys. **69**, 1253 (1991).
[13] S. B. Radovanov, J. K. Olthoff, R. J. Van Brunt, and S. Djurovic, J. Appl. Phys. **78**, 746 (1995).
[14] S. Djurovic and J. R. Roberts, J. Appl. Phys. **74**, 6558 (1993).
[15] T. G. Beuthe and J.-S. Chang, Jpn. J. Appl. Phys., Part 1 **38**, 4576 (1999).
[16] Z. L. Petrovic, S. Bzenic, J. Jovanovic, and S. Djurovic, J. Phys. D **28**, 2287 (1995).
[17] M. Surendra and D. B. Graves, Appl. Phys. Lett. **56**, 1022 (1990).
[18] M. M. Turner, Phys. Rev. Lett. **75**, 1312 (1995).
[19] V. Vahedi and M. Surendra, Comput. Phys. Commun. **87**, 179 (1995).
[20] T. E. Nitschke and D. B. Graves, J. Appl. Phys. **76**, 5646 (1994).
[21] T. J. Sommerer and M. J. Kushner, J. Appl. Phys. **71**, 1654 (1992).
[22] R. W. Boswell and I. J. Morey, Appl. Phys. Lett. **52**, 21 (1988).
[23] T. H. Chung, H. J. Yoon, T. S. Kim, and J. K. Lee, J. Phys. D **20**, 1014 (1996).
[24] G. Gozadinos, D. Vender, M. M. Turner, and M. A. Lieberman, Plasma Sources Sci. Technol. **10**, 117 (2001).
[25] V. V. Ivanov, A. V. Popov, and T. V. Rakhimova, Plasma Phys. Rep. **21**, 692 (1995).
[26] C. Li and C.-H. Wu, IEEE Trans. Plasma Sci. **20**, 1000 (1992).
[27] M. Surendra and D. B. Graves, IEEE Trans. Plasma Sci. **19**, 144 (1991).

[28] V. Vahedi, C. K. Birdsall, M. A. Lieberman, G. DiPeso, and T. D. Rognlien, Plasma Sources Sci. Technol. **2**, 272 (1993).
[29] D. Vender and R. W. Boswell, IEEE Trans. Plasma Sci. **18**, 725 (1990).
[30] E. Kawamura, C. K. Birdsall, and V. Vahedi, Plasma Sources Sci. Technol. **9**, 413 (2000).
[31] C. K. Birdsall and A. B. Langdon, *Plasma Physics via Computer Simulation* (IOP, Bristol, 1991).
[32] V. Vahedi, G. DiPeso, C. K. Birdsall, M. A. Lieberman, and T. D. Rognlien, Plasma Sources Sci. Technol. **2**, 261 (1993).
[33] A. V. Phelps and Z. L. Petrovic, Plasma Sources Sci. Technol. **8**, R21 (1999).
[34] S. J. Buckman and A. V. Phelps, J. Chem. Phys. **82**, 4999 (1985).
[35] H. Tawara, Y. Itakawa, H. Nishimura, and M. Yoshino, J. Phys. Chem. Ref. Data **19**, 617 (1990).
[36] A. V. Phelps, J. Phys. Chem. Ref. Data **21**, 883 (1992).
[37] A. V. Phelps, J. Phys. Chem. Ref. Data **19**, 653 (1990).
[38] T. Tabata and T. Shirai, At. Data Nucl. Data Tables **76**, 1 (2000).
[39] A. V. Phelps (private communication); ftp://jila.colorado.edu/collision_data
[40] B. L. Peko, R. L. Champion, and Y. Wang, J. Chem. Phys. **104**, 6149 (1996).
[41] V. A. Godyak, R. B. Piejak, and B. M. Alexandrovich, Plasma Sources Sci. Technol. **1**, 36 (1992).